



Folic acid and cell-penetrating peptide conjugated PLGA–PEG bifunctional nanoparticles for vincristine sulfate delivery

Jianian Chen^{a,b}, Shaoshun Li^a, Qi Shen^{a,*}

^a School of Pharmacy, Shanghai Jiao Tong University, Dongchuan Road 800, Shanghai 200240, China

^b Key Laboratory for the Chemistry and Molecular Engineering of Medicinal Resources, Guangxi Normal University, Ministry of Education of China, Guilin, Guangxi 541004, China

ARTICLE INFO

Article history:

Received 30 January 2012

Received in revised form 2 July 2012

Accepted 3 July 2012

Available online 10 July 2012

Keywords:

Nanoparticles

PLGA–PEG

Cell-penetrating peptide

Folate

Vincristine sulfate

ABSTRACT

Dual- and multi-functional drug delivery systems, especially ligand-modified nanoparticles (NPs) loaded with chemotherapeutic agents are paid much attention to due to their excellent behavior *in vitro* and *in vivo*. Bifunctional NPs (BF-NPs), which were based on PLGA–PEG and modified with folic acid and cell penetrating peptide R₇ simultaneously, were developed. BF-NPs loaded with vincristine sulfate (VCR) were prepared via the water–oil–water emulsion solvent evaporation method. BF-NPs showed favorable particle size and zeta potentials, promising drug loading and entrapment efficiency. The release of VCR from BF-NPs exhibited a biphasic release manner. Cellular uptake of BF-NPs was found to be higher than that of the NPs merely modified by folic acid or R₇. *In vitro* cytotoxicity, cell apoptosis and cell cycle arrest studies also revealed that BF-NPs were more potent than those of the NPs merely modified by folic acid or R₇. Therefore, the results demonstrated that BF-NPs developed in this study could be a potential vehicle for delivering chemotherapeutic agents such as VCR and breast cancer therapy.

© 2012 Elsevier B.V. All rights reserved.

1. Introduction

Ligand-modified nanoparticle drug delivery systems are paid much attention for their site-specific targeting capacity (van Vlerken et al., 2007; Wang and Thanou, 2010; Wang et al., 2009). Folic acid as a targeting ligand, is extensively used to immobilize on the surface of nano-sized polymeric carriers to deliver these nanoparticles (NPs) into cells mainly via receptor-mediated endocytosis (Barz et al., 2010; Esmaeili et al., 2008). However, the selective permeability of the plasma membrane prohibits most exogenous agents from gaining cellular access. A relatively new research direction that addresses this problem is the introduction of cell-penetrating peptides (CPPs) to overcome the permeability barrier and translocate a variety of cargo including small molecules, nucleic acids, antibodies, and NPs across the plasma membrane (Goncalves et al., 2005; Herbig et al., 2007). Although a complete understanding of the exact mechanism of cellular entry of CPPs remains elusive, its application has been a new avenue for the development of novel drug delivery systems in the past decade (Chugh et al., 2010; Desai et al., 2010; El-Sayed et al., 2009). Several cellular uptake mechanisms have been put forward for CPPs in previous reports: from direct translocation (Patel et al., 2007; Patlolla et al., 2010; Su et al., 2010) to endocytosis (Amand et al., 2008; Richard et al., 2005) as well as the combination of several pathways

(Schmidt et al., 2010). CPPs generally consist of domains of less than 30 amino acids that are rich in basic residues (Torchilin, 2008). Among them, arginine-rich CPPs (e.g., R₆, R₇, and R₉) are widely studied maybe because of their relatively simple structure (Fonseca et al., 2009; Maiolo et al., 2005; Schmidt et al., 2010). The application of CPPs including anticancer drug–CPP conjugation (Aroui et al., 2010), liposome (Marty et al., 2004; Tseng et al., 2002), and micelles (Sethuraman et al., 2008) is more and more attractive to achieve increased tumor penetration by the CPPs and to enhance cellular uptake in tumor cells of the drug.

Vincristine sulfate (VCR), which is a cell cycle-specific anticancer agent, is widely used in cancer chemotherapy. Its cytotoxic activity is based on the ability to inhibit microtubule, altering the tubulin polymerization equilibrium and resulting in altered microtubule structure and function, which then causes arrest of cell division in metaphase (Kassem et al., 2011). Up to now, though multiple novel formulations of VCR, such as liposome, microsphere and nanoparticle, have been studied, most of its formulations are still in the pre-clinical research stage and only conventional formulation–injection is used in clinical (Noble et al., 2009; Bedikian et al., 2011). The principle clinical toxicity of VCR is peripheral neurotoxicity. Neurologic toxicity is usually cumulative and dose-dependent.

Poly(lactic-co-glycolic acid) (PLGA) has generated tremendous interest due to its excellent biocompatibility, biodegradability, and mechanical strength. It has been used extensively for drug delivery or biomaterial applications. Commercial pharmaceutical

* Corresponding author. Tel./fax: +86 21 34204049.

E-mail address: qshen@sjtu.edu.cn (Q. Shen).

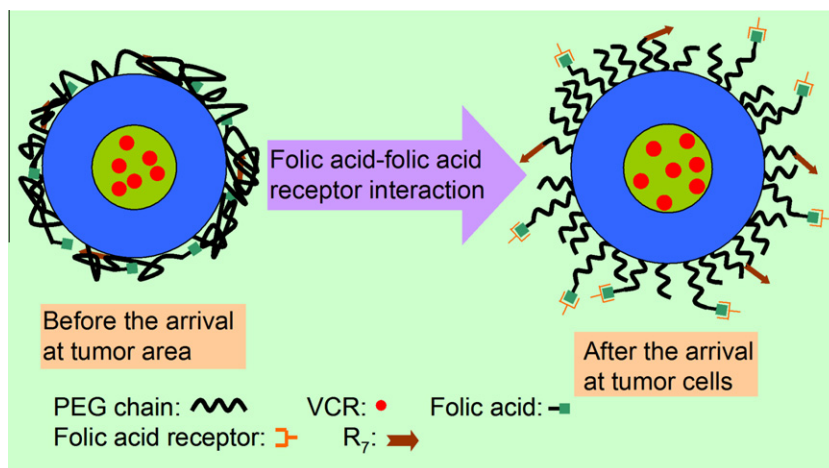


Fig. 1. Schematic diagram depicting the concept of bifunctional nanoparticles (BF-NPs) modified with folic acid and R_7 . R_7 is designed to conjugate at the end of the comparatively shorter PEG chains.

devices include PLGA-based nanoparticles, liposomes, nanocapsules, microspheres and so on (Danhier et al., 2012). But the body recognizes these particles as foreign. The reticulo-endothelial system (RES) easily eliminates these from the blood stream and takes them up in the liver or the spleen. To address these limitations, hydrophilic polymer polyethylene glycol (PEG) is generally modified on the surface of these particles.

The aim of this study is: (1) to construct a novel nanoparticle drug delivery system, PLGA-PEG bifunctional NPs (BF-NPs) which are simultaneously modified with targeting moiety folic acid and cell-penetrating peptide R_7 ; (2) to evaluate *in vitro* at the cellular level by performing the cellular uptake, cytotoxicity, cell apoptosis and cell cycle assay. In detail, PLGA₁₅₀₀₀-PEG₃₃₅₀-folate (abbreviation: PLGA-PEG-folate) and PLGA₁₅₀₀₀-PEG₂₀₀₀- R_7 (abbreviation: PLGA-PEG- R_7) were synthesized, respectively. Based on the polymeric carriers PLGA₁₅₀₀₀-mPEG₂₀₀₀ (abbreviation: PLGA-mPEG), PLGA-PEG-folate, and PLGA-PEG- R_7 , BF-NPs loaded with VCR were prepared via a slightly modified water-oil-water emulsion solvent evaporation method. The *in vitro* release behavior of VCR was studied in Tris-HCl buffer. The cellular uptake of the NPs by the tumor cells MCF-7 was investigated using coumarin 6 as a fluorescence probe. The *in vitro* cytotoxicity of BF-NPs against MCF-7 cells was compared with that of the NPs merely modified with folic acid on the surface (PLGA-PEG-folate NPs), the NPs merely modified with R_7 (PLGA-PEG- R_7 NPs), PLGA-mPEG NPs, and free VCR (F-VCR). The selective cytotoxicity of BF-NPs on MCF-7 cells and normal cells MCF-10A was investigated. Following this, the ability of BF-NPs to induce apoptosis in MCF-7 and MCF-10A cells was evaluated. Finally, the cell cycle arrest of MCF-7 cells by BF-NPs was assayed. By the study of the behavior of BF-NPs *in vitro*, we hope to clarify the correlation of the above three aspects. The introduction of folic acid on the surface of BF-NPs is to achieve active targeting to the tumor cells (Barz et al., 2010); the introduction of the cell penetrating peptide R_7 is to increase penetration power and to improve cellular uptake in tumors of the drug VCR (Herbig et al., 2007; Ziegler et al., 2003). Schematic diagram of the concept is depicted in Fig. 1.

2. Materials and methods

2.1. Materials

For the synthesis of the NPs, PEG-bis-amine (NH_2 -PEG- NH_2 , average molecular weights: 2000 Da and 3350 Da, respectively)

was obtained from Biomatrik Inc. (Jiaxing City, Zhejiang Province, China). Polyvinyl alcohol (PVA, viscosity: 11–14 cp) was obtained from Shanghai Kayon Biological Technology Co., Ltd. (Shanghai City, China). Coumarin 6 and 3-(4,5-dimethylthiazol-2-yl)-2,5-diphenyltetrazolium bromide (MTT) were purchased from Sigma-Aldrich (Missouri, USA). VCR was obtained from Shanghai Anticancer Phytochemistry Co., Ltd. (Shanghai City, China). Poly(lactide-co-glycolide) (PLGA-COOH, 50 mol% of lactide, average Mw 15 kDa), PLGA₁₅₀₀₀-mPEG₂₀₀₀ were purchased from Daigang Corporation (Jinan City, Shandong Province, China). Tris base was obtained from Amresco (Ohio, USA). R_7 - NH_2 (RRRRRRR- NH_2) was synthesized by GL Biochem Ltd. (Shanghai City, China). Folic acid, stannous octoate, *N*-hydroxy-succinimide (NHS), 1,3-diisopropylcarbodiimide (DIC), triethylamine (Et_3N), 4-dimethylaminopyridine (DMAP), succinic anhydride, *N*-hydroxybenzotriazole (HOBt), dimethyl sulfoxide (DMSO), and other reagents were purchased from Aladdin Reagent Co., Ltd. (Shanghai City, China).

For cell culture experiments, human breast cancer cell line (MCF-7) and normal human mammary epithelial cell line (MCF-10A) were purchased from Shanghai Institutes for Biological Sciences (Shanghai City, China). Dulbecco's modified Eagle's medium (DMEM), DMEM/F12 (1:1), fetal bovine serum, horse serum, Hoechst 33342, penicillin-streptomycin, and trypsin-EDTA (0.25% trypsin-0.02% EDTA tetra-sodium) were obtained from Genom Biomedical Technology Co., Ltd. (Shanghai City, China). Insulin, hydrocortisone, cholera toxin, and epidermal growth factor (EGF) were purchased from Sigma-Aldrich (Missouri, USA). BCA protein assay kit and the Annexin V-FITC/propidium-iodide (Annexin V-FITC/PI) apoptosis detection kit were obtained from Nanjing KeyGen Biotech Co. Ltd. (Jiangsu Province, China) and Beijing Biosea Biotechnology Co. Ltd. (Beijing City, China), respectively.

Nuclear Magnetic Resonance (NMR) spectra were recorded on a MERCURY plus 400 instrument (Varian, Inc., California, USA) with TMS as an internal standard. Fourier transform infrared spectroscopy (FTIR) data were acquired at room temperature using an EQUINOX 55 system (Bruker Corp., Karlsruhe, Germany). Nitrogen content in polymers was measured by an elemental analyzer (Elementar Vario EL III, Germany). Particle size and zeta potentials were measured using a 90Plus particle size analyzer (Brookhaven Instruments Corporation, New York, USA). Scanning electron microscope (SEM) images were obtained using a field emission microscope (FEI SIRION 200/INCA OXFORD, USA FEI/UK OXFORD). Three kinds of instruments including Varioskan Flash microplate

reader (Thermo Fisher Scientific, Maryland, USA), FACSCalibur flow cytometer (Becton Dickinson, New Jersey, USA), and TCS SP5 laser scanning confocal microscope (Leica, Solms, Germany) were introduced to study the cellular uptake of the NPs. Olympus IX71 fluorescence microscope (Olympus Corp., Tokyo City, Japan) was used to detect qualitatively the cell apoptosis.

2.2. Synthesis of polymeric carriers: cell-penetrating peptide R₇- and folate-conjugated PLGA-PEG (PLGA-PEG-R₇, PLGA-PEG-folate)

Polymer R₇-conjugated PLGA-PEG (PLGA-PEG-R₇) was synthesized in three steps: (1) synthesis of di-block copolymer PLGA-PEG-NH₂ by coupling NH₂-PEG₂₀₀₀-NH₂ (abbreviation: NH₂-PEG-NH₂) with activated PLGA-COOH; (2) synthesis of PLGA-PEG-succinate by coupling PLGA-PEG-NH₂ with succinic anhydride; and (3) synthesis of PLGA-PEG-R₇ by coupling PLGA-PEG-succinate with R₇-NH₂. In detail, PLGA-COOH (1.5 g, 0.1 mmol) dissolved in dried chloroform (30 mL) was activated by DIC (63 μg, 0.5 mmol) and NHS (57.5 mg, 0.5 mmol) at room temperature under a nitrogen atmosphere for 24 h (PLGA-COOH/NHS/DIC stoichiometric molar ratio: 1/5/5). The activated PLGA-COOH was added slowly to a mixture of dried PEG-bis-amine (0.6 g, 0.3 mmol), DMAP (36.7 mg, 0.3 mmol) and Et₃N (41.8 μL, 0.3 mmol) dissolved in 20 mL of anhydrous chloroform using a syringe while gently stirring. The mixture was agitated for 60 h under nitrogen protection (PLGA-COOH/PEG-bis-amine stoichiometric molar ratio: 1/3). The resultant solution was concentrated and precipitated by dropping it into ice-cold diethyl ether. The precipitated product, amine-terminated di-block copolymer (PLGA-PEG-NH₂), was filtered, dialyzed (MWCO 10,000) against a mixed medium containing water and DMSO (80:20, v/v), and lyophilized. Succinate-conjugated di-block copolymer (PLGA-PEG-succinate) was synthesized by coupling dried PLGA-PEG-NH₂ di-block copolymer with succinic anhydride in the presence of DMAP and Et₃N. Finally, R₇-conjugated PLGA-PEG polymer (PLGA-PEG-R₇) was synthesized via the conjugation of PLGA-PEG-succinate with R₇-NH₂. The synthetic route is shown in Fig. 2. The polymer PLGA-PEG-folate was synthesized according to the method described previously (Yoo and Park, 2004). Briefly, PLGA-PEG-NH₂ (1.84 g, 0.1 mmol) dissolved in 30 mL of DMSO was mixed with folic acid (0.11 g, 0.25 mmol) and DIC (63 μg, 0.5 mmol) and NHS (57.5 mg, 0.5 mmol) at room temperature. The reaction was performed for 18 h and then mixed with 150 mL of distilled water and centrifuged at 3000 rpm. After discarding the pellet, the supernatant was dialyzed and dried. The concentration of conjugated folic acid was determined at 365 nm after the obtained product was dissolved in DMSO.

2.3. VCR NPs

2.3.1. Preparation of VCR-loaded NPs

Because VCR was amphiphilic, we prepared BF-NPs loaded with VCR by water-oil-water emulsion solvent evaporation method with slight modifications (Cohen-Sela et al., 2009; Cun et al., 2010; Meng et al., 2003). Briefly, 1.0 mL of Tris-HCl buffer (pH 6–7.4) containing 10 mg vincristine sulfate was emulsified in 15 mL of ethyl acetate/chloroform (v:v = 1:1) containing 190 mg polymeric carriers (PLGA-mPEG, PLGA-PEG-folate, and PLGA-PEG-R₇, w/w/w = 7:2:1) by sonication over an ice-bath using a Scientz-IID ultrasonic probe (Ningbo Scientz Biotechnology Corp., China) at an output of 90 W for 30 s. The primary emulsion was added to 200 mL of 1.0% (w/v) PVA solution (pH 6–7.4) and sonicated for 2 min to form a double-emulsion. Organic solvent residues were removed by stirring at room temperature and evaporating under reduced pressure. The nanodroplets were centrifuged at 15,000 rpm for 1 h to remove free VCR (F-VCR) in the system. Then the obtained nanoparticle suspension was frozen and lyophilized in a freeze-drier system to obtain the nanoparticle powder. PLGA-mPEG NPs were prepared by similar procedure and only PLGA-mPEG was added instead of the above three kinds of polymeric carriers during the formation of the primary emulsion; PLGA-PEG-folate NPs were prepared using PLGA-mPEG and PLGA-PEG-folate (w/w = 7/2) as the polymeric carriers; and PLGA-PEG-R₇ NPs were prepared using PLGA-mPEG and PLGA-PEG-R₇ (w/w = 7/2) as the polymeric carriers. To investigate the cellular uptake of the NPs, coumarin 6-loaded NPs were similarly prepared via the addition of coumarin 6 during the formation of the primary emulsion.

2.3.2. Characterization of particle size and zeta potential

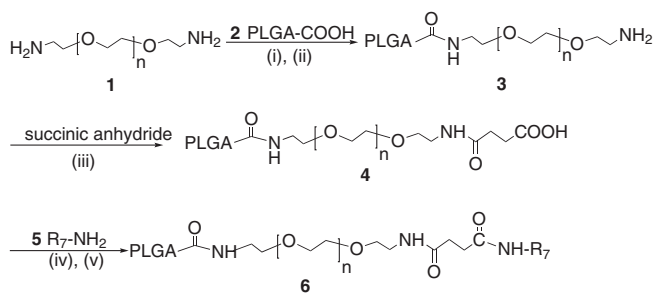
To determine particle size and zeta potential, the nanoparticle suspension was diluted and measured using a particle size analyzer. The samples were analyzed by autocorrelation to determine both mean size and zeta potential. All measurements were performed in triplicate.

2.3.3. Morphology study

The morphological examination of NPs was performed using a field emission scanning electron microscope at an accelerating voltage of 5 kV. A drop of diluted nanoparticle solution sample was placed onto a copper sheet and then dried under reduced pressure at 40 °C. For SEM analysis, the surfaces of the corresponding membranes were sputtered with gold in a vacuum before viewing under the microscope.

2.3.4. Evaluation of drug content

The drug loading and entrapment efficiency of VCR in NPs were determined as follows: 150 mg of dried NPs were evenly dispersed in 15 mL of physiological saline, and final NPs concentration was obtained (10 mg/mL). 10 μL of the sample was removed from the nanoparticle suspension, then 90 μL of DMSO was added to destruct the NPs. After the sample was vortexed for 30 s, 900 μL methanol was added to precipitate insoluble polymers. After the mixture was vortexed again and centrifuged, the supernatant was removed, filtered using a 0.45 μm Millipore filter, and subjected to HPLC analysis to determine the drug concentration. The result is defined as drug concentration encapsulated into the NPs. The mobile phase of the HPLC consisted of a mixture of 0.02 M aqueous dipotassium hydrogen phosphate-methanol (14:86, v/v) at a flow rate of 0.7 mL/min; pH was adjusted to 6.7. The column effluent was detected at 267 nm with a UV-Vis detector (LC20AT Shimadzu, Japan). Finally, according to the following formulae (1) and (2), the drug loading and entrapment efficiency of VCR into NPs



Reaction conditions: (i) DIC, NHS, CHCl₃; (ii) DMAP, Et₃N, CHCl₃;

(iii) DMAP, Et₃N, CHCl₃; (iv) DIC, NHS, DMF; (v) HOBT, DMAP, Et₃N, DMF

Fig. 2. Synthetic pathway for PLGA-PEG-R₇.

could be determined. The measurements were performed in triplicate.

Drug loading (%)

$$= (\text{drug concentration encapsulated into the NPs}) / (\text{the concentration of the final nanoparticle suspension}) \times 100 \quad (1)$$

Entrapment efficiency (%)

$$= (\text{drug concentration encapsulated into the NPs}) / (\text{total drug concentration}) \times 100 \quad (2)$$

In the formulae, total drug concentration can be calculated using the following equation: total drug concentration = (total drug amount added during the process) / (the dispersion volume); the dispersion volume refers to the physiological saline volume (15 mL) where lyophilized NPs are dispersed.

2.4. *In vitro* drug release behavior

To evaluate the *in vitro* release behavior of VCR from BF-NPs in Tris–HCl buffer, a dialysis technique was used. In brief, 2 mL of VCR-loaded BF-NPs suspension was placed in a dialysis bag (MWCO 1000) and dialyzed against the release medium (30 mL) with 100 ± 2 rpm at 37 ± 0.5 °C. At predetermined time intervals (including time zero), 300 μ L of the solution outside the dialysis bag was removed for analysis. Meanwhile, fresh medium was added to replenish the medium which had been partially depleted. The removed samples were immediately frozen and stored at -70 °C until analysis. The samples were detected by HPLC. The percentage of the released VCR from BF-NPs was calculated for every sample from the different incubation periods and presented as a cumulated curve. To compare the release profiles, the release of VCR from PLGA–PEG–folate NPs, PLGA–PEG–R₇ NPs, and F-VCR in the dialysis bag was performed following the same procedure.

2.5. Cell culture and cellular uptake

2.5.1. Cellular uptake study by microplate reader and FACS

The NPs uptake into cultured MCF-7 cells was examined by tracing coumarin 6-labeled NPs using fluorescence microplate reader and flow cytometry. For microplate reader method, MCF-7 cells were seeded in 96-well black plates. After the cells reached 70–80% confluency, the medium in the wells was replaced with 100 μ L of freshly coumarin 6-loaded nanoparticle suspension (the loading rate of coumarin 6 was 0.1%). The concentrations of the NPs in the wells were 100, 200, 400, and 500 μ g/mL, respectively; and the plates were incubated for 1 h. After the suspension was removed, the cells were washed with cold PBS (0.01 M, pH 7.4) three times to eliminate traces of NPs left in the wells. Then 1% Triton X-100 in 0.1 N NaOH was introduced into each well to lyse the cells. The fluorescence intensity of each sample well was measured by microplate reader with excitation wave length at 450 nm and emission wavelength at 510 nm (Zhang et al., 2010). The amount of NPs (μ g) entering into the cells could be determined by the following method: A standard curve for the NPs was constructed by suspending different concentrations of the NPs (80–700 μ g/mL) in 1% Triton X-100 in 0.1 N NaOH followed by lyophilization and extraction of coumarin 6 in methanol. Then the amount of the NPs in the cell lysates (this portion of the NPs entered into the cells) was determined according to the above standard curve. The total cell protein content in each well was determined using BCA protein assay; a standard curve (absorbance–protein concentration, A₅₆₂–C) was obtained with BSA solution. The uptake of the NPs by MCF-7 cells was calculated using the above A₅₆₂–C

standard curve and expressed as the amount of nanoparticles (μ g) uptaken per mg cell protein (Hu et al., 2009). In a separate experiment, to study the effect of receptor-competition on the uptake, the cells were pre-incubated with 20 μ g/mL of folic acid for 1 h at 37 °C, and then incubated with the coumarin 6-loaded NPs suspension (300 μ g/mL) for 0.5, 1, 1.5, 2, and 4 h, respectively. The following steps were the same as described above. To evaluate the function of the cell-penetrating peptide R₇, free R₇ was similarly pre-incubated with the cells. All measurements were performed in triplicate.

For FACS assay, 6-well white plates were used instead of 96-well black plates. After 1×10^6 cells were co-incubated with coumarin 6-loaded NPs, MCF-7 cells were harvested. Then the cells were washed twice with PBS and analyzed in a flow cytometer. For each sample, 1×10^4 cells were collected.

2.5.2. Confocal laser scanning microscopy

To study the localization of NPs within MCF-7 cells, a total of 1×10^6 cells were seeded on a 6-well white plate and allowed to attach overnight. Then the cells were incubated with the suspension of BF-NPs simultaneously loaded with VCR (5 nM) and coumarin 6 (300 ng/mL) for different time at 37 °C. The adherent cells were digested and merged with the floating fraction. The cells were washed with PBS for three times to eliminate the NPs which did not enter into the cells, and then fixed by 2% paraformaldehyde in PBS for 15 min. They were further washed twice with PBS and the nuclei were stained by incubating with PI for another 15 min. The cells were re-suspended in 50 μ L fresh PBS with 10 μ L antifade mounting medium. 10 μ L of suspension containing cells was removed and placed on a clean glass to be observed by a confocal laser scanning microscope (CLSM).

2.6. *In vitro* cytotoxicity by MTT assay

MTT method was used to evaluate the cytotoxicity of BF-NPs. In 96-well plates, MCF-7 cells were seeded at a density of 5×10^4 cells/mL, then cultivated at 37 °C for 8 h. DMEM was replaced by 100 μ L fresh medium containing BF-NPs. After co-incubation for 24 h, 20 μ L of MTT solution in PBS (5 mg/mL) was added to each well, and the cells were incubated for another 4 h at 37 °C in the darkness. After drawing-off of the culture medium, 100 μ L DMSO was added to dissolve formazan crystal; the percentage of cell viability was determined using a microplate reader. F-VCR, PLGA–mPEG NPs, PLGA–PEG–folate NPs, and PLGA–PEG–R₇ NPs were performed following the same procedure to compare their cytotoxicities. In order to evaluate the harmfulness of VCR NPs on normal cells, human mammary epithelial cell line MCF-10A was chosen and the selectivity index (SI) was determined (Mena-Rejon et al., 2009). The SI was calculated from the IC₅₀ values of normal cells MCF-10A and tumor cells MCF-7 [SI = (IC₅₀ of MCF-10A cells) / (IC₅₀ of MCF-7 cells)]. SI value indicates the selectivity of the sample to the cell lines tested. The IC₅₀ values are defined as the drug concentrations that kill 50% of cells relative to the controls. All assays were conducted with four parallel samples.

2.7. Evaluation of cell apoptosis

The apoptotic induction of MCF-7 cells by BF-NPs, PLGA–PEG–folate NPs, PLGA–PEG–R₇ NPs, or F-VCR was measured quantitatively by Annexin V binding assay (Nahar et al., 2010). Briefly, MCF-7 cells in 6-well plates were co-incubated with VCR formulations at 37 °C for 12 h. Then the cells floating in the supernatant were combined with the adherent fraction and washed with PBS three times. The cells were incubated with Annexin V-FITC and PI for another 15 min at room temperature in the darkness according to the manufacturer's instructions, and immediately analyzed

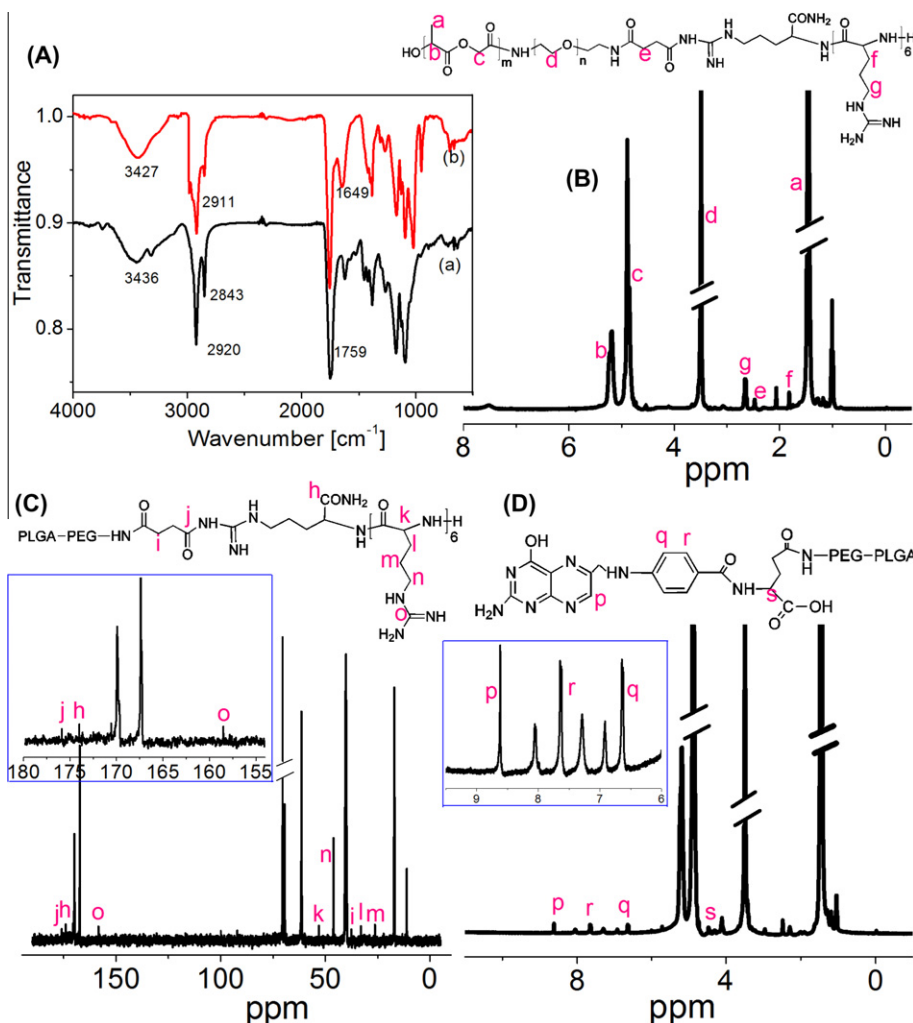


Fig. 3. Infrared spectra of the synthesized polymers (A). (a) and (b) represent PLGA-PEG-folate and PLGA-PEG- R_7 , respectively. The presence of all major vibrational features associated with PLGA, PEG, folate, and R_7 can be seen in the spectra. ^1H NMR (B) and ^{13}C NMR (C) of the polymer PLGA-PEG- R_7 . ^1H NMR of the polymer PLGA-PEG-folate (D).

in a flow cytometer. The percentages of viable (Annexin V-/PI-), early apoptotic (Annexin V+/PI-), late apoptotic or secondary necrotic (Annexin V+/PI+), and necrotic (Annexin V-/PI+) cells were determined using CellQuest software (Becton Dickinson). For each sample, 1×10^4 cells were collected.

To evaluate whether VCR NPs were capable of inducing apoptosis in normal cells, the apoptotic morphology of MCF-7 and MCF-10A cells was compared by Hoechst 33342/PI dual staining method (Shimazawa et al., 2007). Briefly, the cells seeded in 24-well plates (5×10^4 cells/well) were co-incubated with VCR loaded PLGA-PEG NPs (10 nM) for 12 h and the following steps were the same as described above. The final concentrations of the fluorescent DNA-binding dyes Hoechst 33342 and PI added to each well were 10 and 4 $\mu\text{g}/\text{mL}$, respectively. For each sample, over 500 cells were analyzed under a fluorescence microscope.

2.8. Cell cycle analysis

Cell cycle distributions in cells were determined by PI staining, which was described previously (Skladanowski et al., 2005). In brief, exponentially growing MCF-7 cells (10^6 per treatment) were treated with F-VCR or VCR NPs suspension for 24 h. Cells treated with culture medium (untreated with VCR formulations) served as the negative control. After cells were trypsinized, washed twice with PBS, and fixed in 70% ethanol for 8 h at 4 $^\circ\text{C}$, they were

washed again with PBS, incubated with Ribonuclease A (50 $\mu\text{g}/\text{mL}$ final concentration) for 30 min at 37 $^\circ\text{C}$, and stained with propidium iodide (50 $\mu\text{g}/\text{mL}$ final concentration) at 4 $^\circ\text{C}$ for 15 min in the darkness. The cell cycle was measured using the above flow cytometer, and the DNA histogram was analyzed using ModFit software. All assays were conducted with three parallel samples. For each sample, 1×10^4 cells were collected.

2.9. Statistical analysis

Values were processed using Microsoft Excel 2003 software and presented as mean \pm SD. Statistical analyses were performed using an unpaired, two tailed student *t*-test. The level of significance was set at $*p < 0.05$.

3. Results and discussion

3.1. Synthesis of polymeric carriers: PLGA-PEG- R_7 and PLGA-PEG-folate

The synthesis of polymer PLGA-PEG- NH_2 can be accomplished by one-pot method: The activated PLGA-COOH need not be separated before the addition of PEG-bis-amine in CHCl_3 . In the succeeding step, with the help of the catalyst, the cycle of succinic anhydride was opened and conjugated to PLGA-PEG- NH_2 . In the

last step, the guanidine in the chain of the oligopeptide R₇ was reacted with PLGA–PEG–succinate and the final product PLGA–PEG–R₇ was obtained. Nitrogen content in the polymer PLGA–PEG–R₇ was 0.74%. On the basis of the method described previously (Yoo and Park, 2004), the polymeric carrier PLGA–PEG–folate was synthesized. PLGA–PEG–folate and PLGA–PEG–R₇ were characterized using FTIR, as depicted in Fig. 3A. To the infrared spectrum of the polymer PLGA–PEG–R₇, the broad bands ranging from 3650 to 3200 cm⁻¹ correspond to the presence of multiple NH₂ groups of the oligomer R₇ and OH groups of PLGA unit; and in many cases, their bands are overlapped. A series of peaks between 3050 and 2800 cm⁻¹ indicate the C–H stretching which are corresponding to multiple methylene groups in PEG chain. Considering R₇ was conjugated at the end of PLGA–PEG–succinate, the presence of a slightly salient peak at 1649 cm⁻¹ could be attributed to the formation of amide bond between amino group and carboxyl group. PLGA shows a prominent peak at 1759 cm⁻¹ corresponding to C=O stretching in the polymers. To further verify the structure of the conjugation, NMR technique was used. A typical ¹H NMR spectrum of PLGA–PEG–R₇ is shown in Fig. 3B. The characteristic signals appearing at 1.82, 2.66 ppm are assigned to the two different groups of methylene hydrogens of R₇ unit. The peak at 2.53 ppm is assigned to the methylene hydrogen of succinyl group. The peaks appearing at 5.08–5.35, 4.71–5.06, 3.39–3.61, and 1.35–1.63 ppm are assigned to the methine hydrogen of the lactide units, methylene hydrogen of the glycolide units, the methylene hydrogen of the PEG, and the methyl hydrogen of the lactide units, respectively. The peak of methine hydrogen of R₇ unit is covered into the multiple peaks of glycolide units (3.39–3.61 ppm). The structure of PLGA–PEG–R₇ was further determined by ¹³C NMR spectrum which was shown in Fig. 3C. The peak at 158.3 ppm is assigned to the guanidinium group carbon of R₇ unit. The peaks appearing at 26.5, 32.7, and 46.0 ppm are assigned to the different methylene carbons of R₇ unit. These results confirm successful conjugation of R₇ to PLGA–PEG. The conjugation percentage of R₇ to PLGA–PEG was 35.7% at the detection wavelength 362 nm. ¹H NMR spectra of the synthesized PLGA–PEG–folate were shown in Fig. 3D, and the conjugation percentage of folate to PLGA–PEG was 39.8%.

3.2. Preparation and characterization of NPs loaded with VCR

We used the water–oil–water emulsion solvent evaporation method (Cohen-Sela et al., 2009; Cun et al., 2010; Meng et al., 2003) and successfully prepared PLGA–mPEG NPs, PLGA–PEG–folate NPs, PLGA–PEG–R₇ NPs, and BF-NPs. It has been reported that at pH below 4.5, the drug entrapment efficiency and drug loading of VCR into liposome are dramatically reduced (Noble et al., 2009). Bearing this in mind, 6–7.4 was chosen as an optimal range of pH values. Unfortunately, the pH values of the nanoparticle emulsions containing PVA and PLGA were below 5.0, it was necessary to add weak alkali to adjust the pH values. According to the previous reports (Marinina et al., 2000; Zhu et al., 2000), the addition of a kind of weak alkaline or anti-acid, such as magnesium hydroxide or basic zinc carbonate, can overcome this obstacle, but a significant increase in particle size was observed because of very low water solubility of these bases. Finally, a PVA aqueous solution (1.0%, w/v) was selected (its pH value was adjusted by Tris–HCl buffer to 6–7.4) and satisfactory results were obtained. It was found that the content of PVA had an important effect on the particle size of the emulsion (Table 1). When PVA was below 0.4%, the NPs easily aggregated and the particle size was large (>350 nm); between 0.4% and 1.0% (w/v), the mean diameter of NPs decreased with the increase of PVA concentration. However, the size gradually increased when the content of PVA continued to increase, maybe due to the increased viscosity of the emulsion. The physical character-

Table 1

Characterization of VCR-loaded NPs (PLGA–PEG–folate NPs, PLGA–PEG–R₇ NPs, and BF-NPs).

Group	Content of PVA (% w/v)	Particle size (nm)	Zeta potential (mV)	Drug loading (%) ^a	Entrapment efficiency (%) ^a
BF-NPs	1.0	247.2 ± 6.2	-12.37 ± 2.62	2.06 ± 0.28	45.22 ± 4.35
PLGA–PEG–folate NPs	1.0	224.5 ± 8.9	-13.06 ± 2.55	2.09 ± 0.26	46.43 ± 4.23
PLGA–PEG–R ₇ NPs	1.0	235.8 ± 11.8	-8.56 ± 1.29	2.02 ± 0.29	43.33 ± 4.56

Data presented as mean ± SD (n = 3).

^a Data on the drug loading and entrapment efficiency are shown only under optimal conditions (the content of PVA was 1.0%, w/v).

istics of VCR-loaded NPs including the particle size, zeta potentials, the drug loading, and drug entrapment efficiency are shown in Table 1. The sizes of NPs were determined by a dynamic laser scattering method and every sample was measured three times. Under optimal conditions, the particle size increased from 224.5 ± 8.9 nm (PLGA–PEG–folate NPs) to 247.2 ± 6.2 nm (BF-NPs); and the zeta potentials of the three kinds of NPs were satisfactory (below -8 mV). There were no significant differences in drug loading and entrapment efficiency among PLGA–PEG–folate NPs, PLGA–PEG–R₇ NPs, and BF-NPs. The SEM images showed that the morphologies of the prepared three kinds of the NPs loaded with VCR (PLGA–PEG–folate NPs, PLGA–PEG–R₇ NPs, and BF-NPs) were similar with a typical spherical shape; and in Fig. 4 only the morphology of BF-NPs was shown.

Following this, the stability of the obtained four kinds of nanoparticles was investigated. At room temperature or at 4 °C within a week, the lyophilized form showed excellent stability, and only 4–7% of VCR leaked from the nanoparticles. Moreover, the lyophilized form of the nanoparticles was more stable than its aqueous solution at the same temperature. Within a week, over 80% of the initial amount of VCR leaked from the nanoparticles if the nanoparticles were kept in aqueous solution at 37 °C. So, freeze-dried powder of the above VCR nanoparticles including BF-NPs was a favorable formulation with excellent stability.

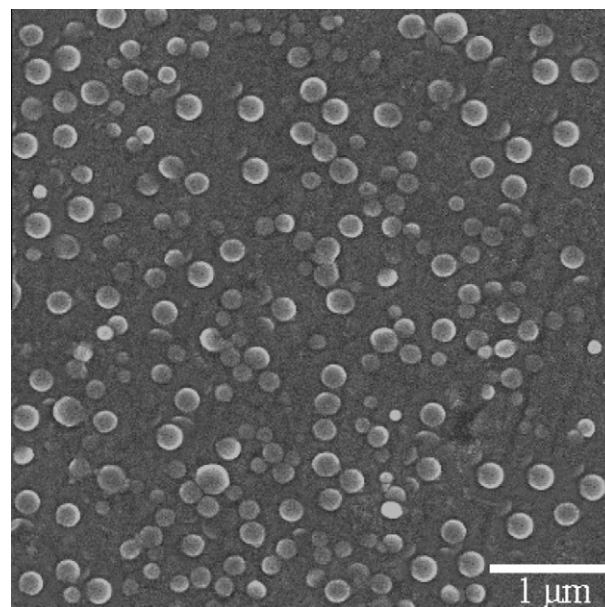


Fig. 4. Scanning electron micrograph of BF-NPs loaded with VCR. Before viewing under the microscope, the surfaces of corresponding membranes were sputtered with gold.

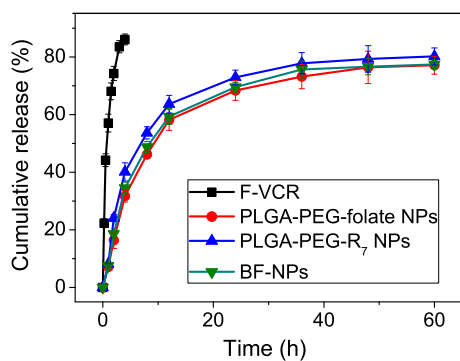


Fig. 5. *In vitro* drug release profiles of VCR from the NPs at 37 °C in Tris-HCl buffer solution (pH 7.4). Data presented as mean \pm SD ($n = 3$).

3.3. *In vitro* release

The *in vitro* release of VCR from the NPs was performed in Tris-HCl buffer (pH 7.4) at 37 ± 0.5 °C. As shown in Fig. 5, over 85% VCR was released from F-VCR solution within 4 h indicating that VCR was released very fast in Tris-HCl buffer. Different from F-VCR, the release of VCR from PLGA-PEG-folate NPs, PLGA-PEG- R_7 NPs, and BF-NPs exhibited a similar process that began with an initial burst release followed by a steady, continued-release pattern. Release was fast in the first 8 h, that is, $46.20 \pm 1.09\%$, $53.67 \pm 2.11\%$, and $48.77 \pm 1.83\%$ VCR release from PLGA-PEG-folate NPs, PLGA-PEG- R_7 NPs, and BF-NPs, respectively. In the following time, a sustained release rate was observed. Within 24 h, the accumulative release was $68.35 \pm 3.43\%$ for PLGA-PEG-folate NPs, $72.91 \pm 2.54\%$ for PLGA-PEG- R_7 NPs, and $69.55 \pm 1.64\%$ for BF-NPs, respectively. The initial burst may be due to the rapid release of drugs deposited on the surface and in the relatively shallow channels of the NPs, whereas the steady release may be

attributed to the diffusion of the drug localized in the PLGA core of the NPs.

3.4. *In vitro* cellular uptake

The NPs labeled with fluorescent dyes are widely used to study the cellular uptake because the uptake can be detected qualitatively by fluorescence microscopy and CLSM, and quantitatively by fluorescence microplate reader, flow cytometry and fluorescence spectrophotometer (Gan and Feng, 2010). In this study, coumarin 6 is chosen as a fluorescence probe (Davda and Labhassetwar, 2002). It is noted that, the entrapment efficiency of coumarin 6 (loading rate: 0.1%) loaded into PLGA-PEG NPs (including PLGA-mPEG NPs, PLGA-PEG-folate NPs, PLGA-PEG- R_7 NPs, and BF-NPs) is very high maybe due to its very low hydrophilicity. In the experiment, it was found that the entrapment efficiency was over 97% in the PLGA-PEG NPs. Moreover, the release of coumarin 6 from the PLGA-PEG NPs was very slow, and within 24 h, the cumulative release was less than 5% (the release curve of coumarin 6 from the NPs was not shown). These results were agreed with the previous report (Win and Feng, 2005). This suggests that the use of coumarin 6 to determine the cellular uptake of the PLGA-PEG NPs is appropriate. We loaded coumarin 6 into the NPs to compare the cellular uptake of BF-NPs, PLGA-mPEG NPs, PLGA-PEG-folate NPs, and PLGA-PEG- R_7 NPs by MCF-7 cells. A time- and concentration-dependent internalization was observed (Fig. 6). Within the low concentration range (100–420 $\mu\text{g}/\text{mL}$, here refers to the concentration of the NPs), there was a difference among the four kinds of NPs, the uptake efficiency order of the coumarin 6-loaded NPs: BF-NPs > PLGA-PEG- R_7 NPs > PLGA-PEG-folate NPs > PLGA-mPEG NPs. However, when the concentration of the NPs added to the wells continued to increase, the difference of the cellular uptake in MCF-7 cells among the four kinds of the NPs became smaller and smaller (Fig. 6A). Compared to PLGA-mPEG NPs without folic acid modification (the first column),

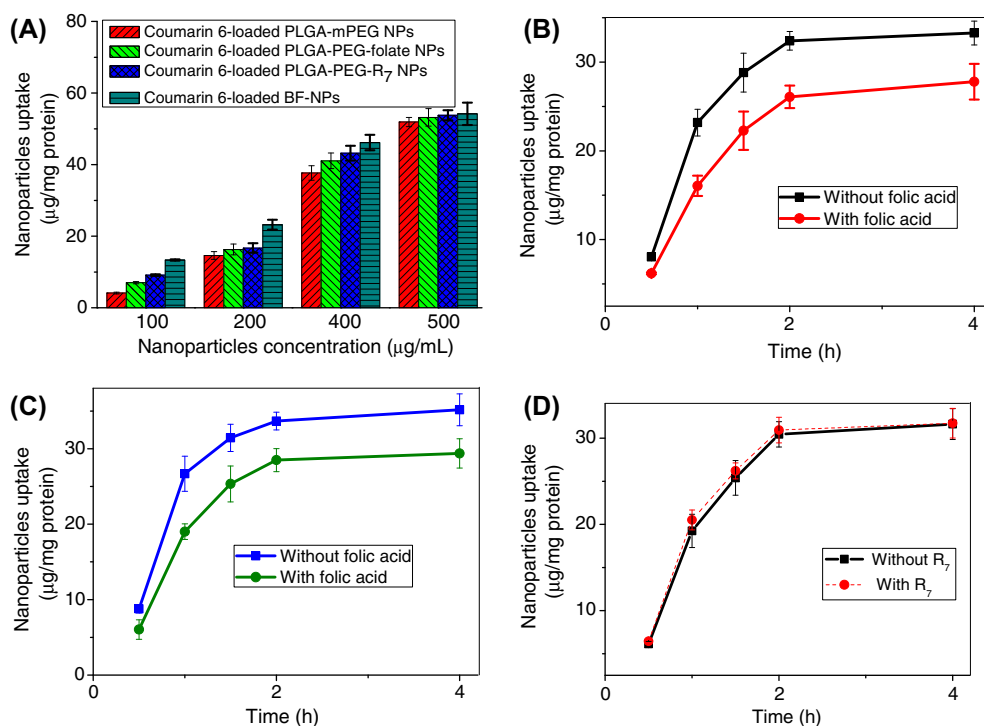


Fig. 6. The cellular uptake by MCF-7 cells of coumarin 6-loaded NPs. Effect of the NPs concentration on the cellular uptake (A). Effect of the pre-incubation by free folic acid on the cellular uptake of PLGA-PEG-folate NPs (B) and BF-NPs (C). Effect of the pre-incubation by free R_7 on the cellular uptake of PLGA-mPEG NPs (D). Data presented as mean \pm SD ($n = 3$).

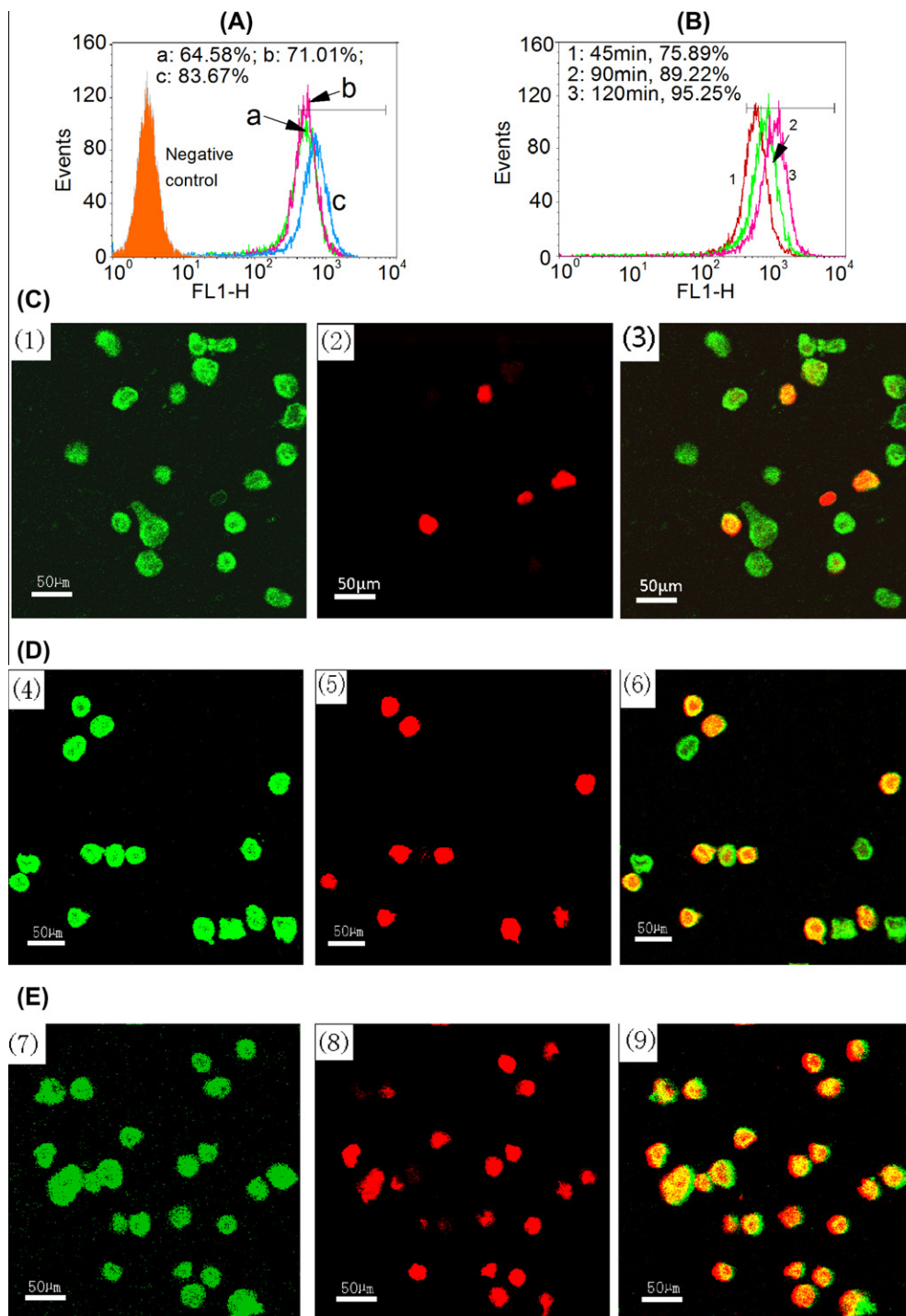


Fig. 7. The cellular uptake of coumarin 6-loaded NPs by MCF-7 cells using FACS analysis (A and B). Confocal microscopic images of MCF-7 cells incubated with coumarin 6-loaded BF-NPs for 0.5, 1, and 4 h at 37 °C, respectively (C–E). In figure (A), a, b, and c represent the cellular uptake profiles of coumarin 6-loaded PLGA–PEG–folate NPs, PLGA–PEG–R₇ NPs, and BF-NPs, respectively. In figure (B), MCF-7 cells were incubated with coumarin 6-loaded BF-NPs for 45, 90, 120 min, respectively. In CLSM assay, the cells were stained with PI (red) and the uptake of fluorescence coumarin 6-loaded BF-NPs (green) in MCF-7 cells was visualized by overlaying images obtained by FITC filter and PI filter: (3), (6), and (9)—images from combined PI channel and FITC channel; (1), (4), and (7)—images from FITC channel; (2), (5), and (8)—images from PI channel. (For interpretation of the references to color in this figure legend, the reader is referred to the web version of this article.)

enhanced uptake of PLGA–PEG–folate NPs (the second column) and BF-NPs (the fourth column) by MCF-7 cells was observed within the range of 100–420 $\mu\text{g}/\text{mL}$. This may be associated with the surface modification: In MCF-7 cells, folic acid receptor is over-expressed. After folic acid is modified on the surface of the NPs, the obtained PLGA–PEG–folate NPs and BF-NPs possess high affinity to the folic acid receptor, which allows the NPs to be easily taken

up by the tumor cells where the folic acid receptor is highly expressed (Stella et al., 2007; Wu et al., 2010). Moreover, the enhanced uptake leads to longer retention time of coumarin 6-loaded PLGA–PEG–folate NPs and BF-NPs within the cells. However, at higher concentrations (>420 $\mu\text{g}/\text{mL}$), the intracellular uptake of coumarin 6 is close to saturation and its concentration within the cells does not significantly increase. We also found that, if

the incubation period was beyond 4 h, there was no significant increase in the cellular uptake of coumarin 6 by MCF-7 cells. These results suggested that there was a saturated uptake phenomenon, which was consistent with the previous report (Win and Feng, 2005). To verify the endocytosis mechanism of BF-NPs and PLGA-PEG-folate NPs partly mediated by folic acid receptor (Yang et al., 2010a), excess free folic acid (20 $\mu\text{g}/\text{mL}$) was added to the wells and pre-incubated with MCF-7 cells for different time. The results were shown in Fig. 6B and C. Compared to that of untreated group, the cellular uptake of PLGA-PEG-folate NPs and BF-NPs evidently declined possibly because the endocytosis of the NPs by MCF-7 cells was partially suppressed.

To investigate the function of R_7 , PLGA-PEG- R_7 NPs loaded with coumarin 6 were prepared which were merely modified with R_7 , and the uptake of coumarin 6 in MCF-7 cells was shown in the third column of Fig. 6A. It was found that, at the same concentration of coumarin 6, the uptake efficiency of PLGA-PEG- R_7 NPs was higher than that of PLGA-PEG-folate NPs and PLGA-mPEG NPs. This result indirectly suggested that R_7 indeed possessed the strong cell-penetrating power. In another separate experiment, the cells were pre-incubated with free R_7 (20 $\mu\text{g}/\text{mL}$) for 1 h at 37 °C, then incubated with the coumarin 6-loaded PLGA-mPEG NPs suspension (300 $\mu\text{g}/\text{mL}$) for 0.5, 1, 1.5, 2, and 4 h, respectively. As shown in Fig. 6D, there was no obvious increase in the cellular uptake of the NPs by MCF-7 cells. The coumarin 6-loaded PLGA-mPEG NPs suspension and free R_7 were simultaneously added to the wells and then co-incubated with the cells for different time, there was also no obvious increase in the cellular uptake of the NPs. In our opinion, though free R_7 possesses strong cell penetration power, it cannot translocate the PLGA-PEG NPs across the plasma membrane because it is independent of the NPs, only the portion of R_7 conjugated on the surface of the NPs can translocate the NPs and then enter into the cells.

Fluorescence levels were also measured quantitatively 1 h post treatment by FACS analysis using FITC channel (Fig. 7A and B). As shown in Fig. 7A, the addition of coumarin 6-loaded PLGA-PEG NPs to MCF-7 cells led to an immediate fluorescence shift, compared with the negative control (without the treatment of VCR formulations). The uptake of BF-NPs increased significantly (profile c, 83.67%), compared to that of PLGA-PEG-folate NPs (profile a, 64.58%) and PLGA-PEG- R_7 NPs (profile b, 71.01%). Consistent with the results of microplate reader assay, the fluorescence intensity in the cells treated with coumarin 6-loaded BF-NPs is time-dependent (Fig. 7B). To study the intracellular localization of VCR-loaded NPs, we simultaneously loaded coumarin 6 and VCR into BF-NPs. As shown in Fig. 7C–E, after MCF-7 cells were co-incubated with the NPs for 0.5 h, an obvious green fluorescence in the cell cytoplasm and red fluorescence around the nucleus were observed. Moreover, the red fluorescence intensity increased with the increase of the incubation time in the first 4 h; When the cells were treated with the NPs for 4 h, the proportion of cells with red fluorescent was much higher than that for 1 h; and a minimum number of MCF-7 cells with red fluorescence were observed when the incubation was only 0.5 h. These results reflected the continuous penetration of NPs into the cells. So we speculate that, bifunctional nanoparticulate carriers probably translocate VCR across the cell membrane by folic acid receptor-mediated endocytosis combining with strong cell-penetrating power, and then enter effectively into the cells.

3.5. *In vitro* assessment of selective cytotoxicity

The *in vitro* cytotoxic activity of BF-NPs was investigated and compared with that of other VCR formulations by MTT assay. After a 24-h exposure of the cells to the VCR formulations, a dose-dependent reduction in growth rate was observed. There was a significant

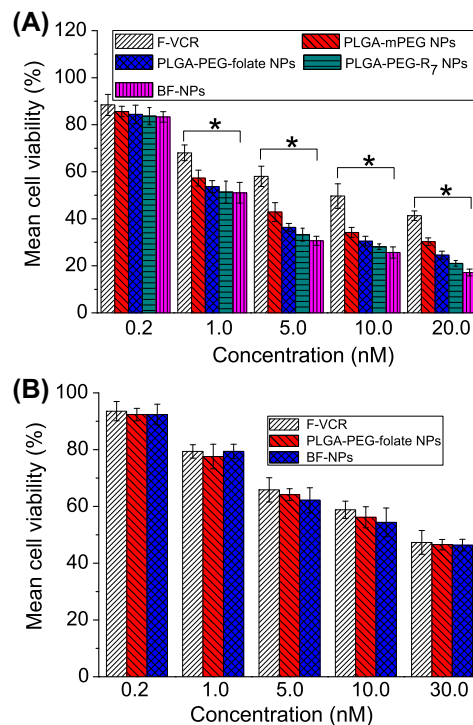


Fig. 8. *In vitro* cytotoxicity determination using MTT assay on MCF-7 (A) and MCF-10A cells (B). The cell lines were co-incubated with VCR-loaded NPs or F-VCR at 37 °C for 24 h. Statistical differences were evaluated using Student's test analysis of variance (ANOVA). Data presented as mean \pm SD ($n = 4$). * $p < 0.05$.

difference in cell viabilities between F-VCR group and the NPs groups. At the same concentration, VCR-loaded BF-NPs showed higher cytotoxicity than did VCR other formulations; the order of the cytotoxicity was BF-NPs > PLGA-PEG- R_7 NPs > PLGA-PEG-folate NPs > PLGA-mPEG NPs > F-VCR. The percent viabilities of MCF-7 cells treated with VCR formulations at different concentrations were shown in Fig. 8A. When the concentration of VCR was 5 nM, the percent viabilities were $42.86 \pm 4.01\%$ for PLGA-mPEG NPs, $36.36 \pm 1.64\%$ for PLGA-PEG-folate NPs, $33.25 \pm 2.77\%$ for PLGA-PEG- R_7 NPs, and $30.65 \pm 1.92\%$ for BF-NPs, respectively. As shown in Table 2, the IC_{50} values decreased from 10.24 ± 1.52 nM for F-VCR to below 4 nM for VCR-loaded NPs, and BF-NPs had the lowest IC_{50} value of 2.07 ± 0.13 nM.

In tumor therapy, it is very important to deliver drugs selectively to tumor cells and minimize the damage on normal cells. So, the selective cytotoxicities of VCR NPs against the normal cells MCF-10A and the tumor cells MCF-7 were compared *in vitro*. There was a significant difference in the sensitivity of the above two cell lines to BF-NPs. The percent viabilities of MCF-10A cells treated

Table 2

Cytotoxic activity and selectivity index of VCR formulations on human breast cancer cells MCF-7 and normal mammary cells MCF-10A.

Groups	IC_{50} (nM) ^a		Selectivity index ^b
	MCF-7 cells	MCF-10A cells	
F-VCR	10.24 ± 1.52	19.71 ± 1.79	1.92
PLGA-mPEG NPs	3.99 ± 0.23	ND ^c	ND ^c
PLGA-PEG-folate NPs	2.76 ± 0.22	$19.16 \pm 1.56^{**}$	6.94
PLGA-PEG- R_7 NPs	2.40 ± 0.19	ND ^c	ND ^c
BF-NPs	2.07 ± 0.13	$18.74 \pm 1.67^{**}$	9.05

^a IC_{50} values presented as mean \pm SD ($n = 4$).

^b Selectivity index is calculated by dividing the IC_{50} obtained from the MCF-10A data (the mean value) by the IC_{50} obtained from the MCF-7 data (the mean value).

^c ND: not determined.

** $p < 0.01$ versus IC_{50} values of VCR NPs against MCF-7 cells.

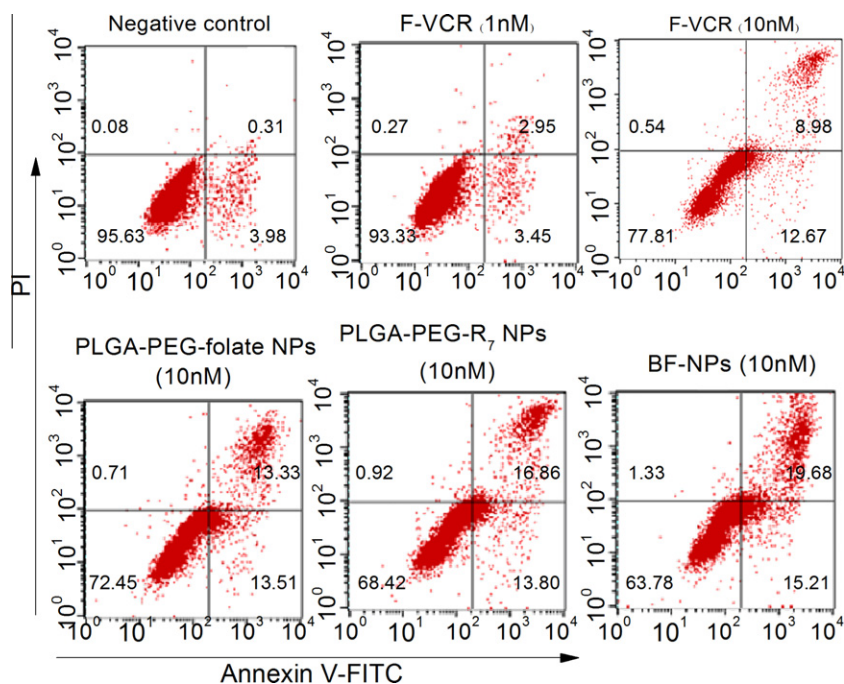


Fig. 9. Quantitative apoptosis assay of MCF-7 using a flow cytometer. MCF-7 cells were incubated with F-VCR or NPs for 12 h. Then the cells were harvested and stained with the Annexin V/PI. Viable cells are shown in the lower-left quadrant (Annexin V⁻, PI⁻). The early and late apoptotic cells are shown in the lower-right quadrant (Annexin V⁺, PI⁻) and upper-right quadrant (Annexin V⁺, PI⁺), respectively.

with F-VCR, PLGA-PEG-folate NPs, and BF-NPs at different concentrations were shown in Fig. 8B. It was found that the NPs displayed comparatively low cytotoxicity against MCF-10A cells; and at the same concentration of VCR, there was no significant difference ($p > 0.05$) in cell viabilities between the control group (F-VCR) and the nanoparticle groups. The IC_{50} values of MCF-10A were more than 18 nM and the selectivity indexes were 1.92 (for F-VCR), 6.94 (for PLGA-PEG-folate NPs), and 9.05 (for BF-NPs), respectively (Table 2). From these results, it was suggested that BF-NPs could selectively exerted their cytotoxic effect on tumor cells MCF-7. The three formations showed no significant toxicity to human normal mammary epithelial cells, which further confirmed the safety to normal cells (Wang et al., 2012).

As mentioned above, the use of CPPs as intracellular delivery vectors has been widely accepted due to their strong cell-penetrating power. Although the mechanism of the arginine-rich CPPs transporting NPs across cell membranes is not yet fully understood, many scientists have already realized the structural properties of cationic arginine-rich CPPs and interactions with membrane phospholipids play a major role in the cellular uptake mechanism (Su et al., 2010). In previous experiments, it was found that, these peptides strongly bound electrostatically to the anionic lipids on the cell membrane (Herbig et al., 2007; Ziegler et al., 2003). Moreover, the guanidinium residues of arginine in arginine-rich CPPs played a fundamental role during translocation not only in the binding of the peptide to the surface of the cell membrane, but also in the destabilization and nucleation of transient pores across the phospholipid bilayer (Herce et al., 2009; Thoren et al., 2005). The results also demonstrate that the cytotoxicity of nanoparticles to cancer cells was improved by the folate component, which has been reported to bind to folate receptors with high affinity, thus mediating in cellular uptake (Wang et al., 2011).

3.6. Apoptosis assay

To quantitatively determine whether the NPs-mediated cell growth inhibition was related to the induction of apoptosis, Annex-

in V and PI dual staining method was used, which could detect both early and late stages of apoptosis. The results were shown in Fig. 9 and Table 3. It was demonstrated that viable cells treated with VCR decreased in a dose-dependent manner. At the same concentration (10 nM), an obvious decrease in viable cells was shown by PLGA-PEG-R₇ NPs (68.42%) and BF-NPs (63.78%), compared with PLGA-PEG-folate NPs (72.45%), the free drug (77.81%), and negative control (95.63%). Concurrently, an obvious increase in apoptotic cells (early plus late apoptotic cells) was detected in MCF-7 cells by PLGA-PEG-R₇ NPs (30.66%) and BF-NPs (34.89%), compared with PLGA-PEG-folate NPs (26.84%) and negative control (4.29%). These results indicated that the above three kinds of the NPs displayed stronger induction of apoptosis than did F-VCR at the same concentration, and BF-NPs exhibited the strongest apoptotic induction in MCF-7 cells.

To evaluate whether BF-NPs were capable of inducing apoptosis in normal cells, the apoptotic morphology of MCF-7 and MCF-10A cells was compared after the cells were treated with VCR NPs. Fluorescence images of the cells stained with Hoechst 33342/PI were showed in Fig. 10. When MCF-7 cells were co-incubated with VCR NPs (10 nM) for 12 h, a large number of cells demonstrated apoptotic features such as nuclear shrinkage, chromatin condensation, or fragmentation. Intensive red fluorescence was observed

Table 3
Effects of F-VCR and nanoparticle formulations on apoptotic induction in MCF-7 cells.

Group	C (nM) ^a	Viable cells (%)	Early apoptotic + late apoptotic cells (%)
Negative control	0	95.63	4.29
F-VCR	1	93.33	6.40
	10	77.81	21.65
PLGA-PEG-folate NPs	10	72.45	26.84
PLGA-PEG-R ₇ NPs	10	68.42	30.66
BF-NPs	10	63.78	34.89

^a Here refers to the concentration of VCR.

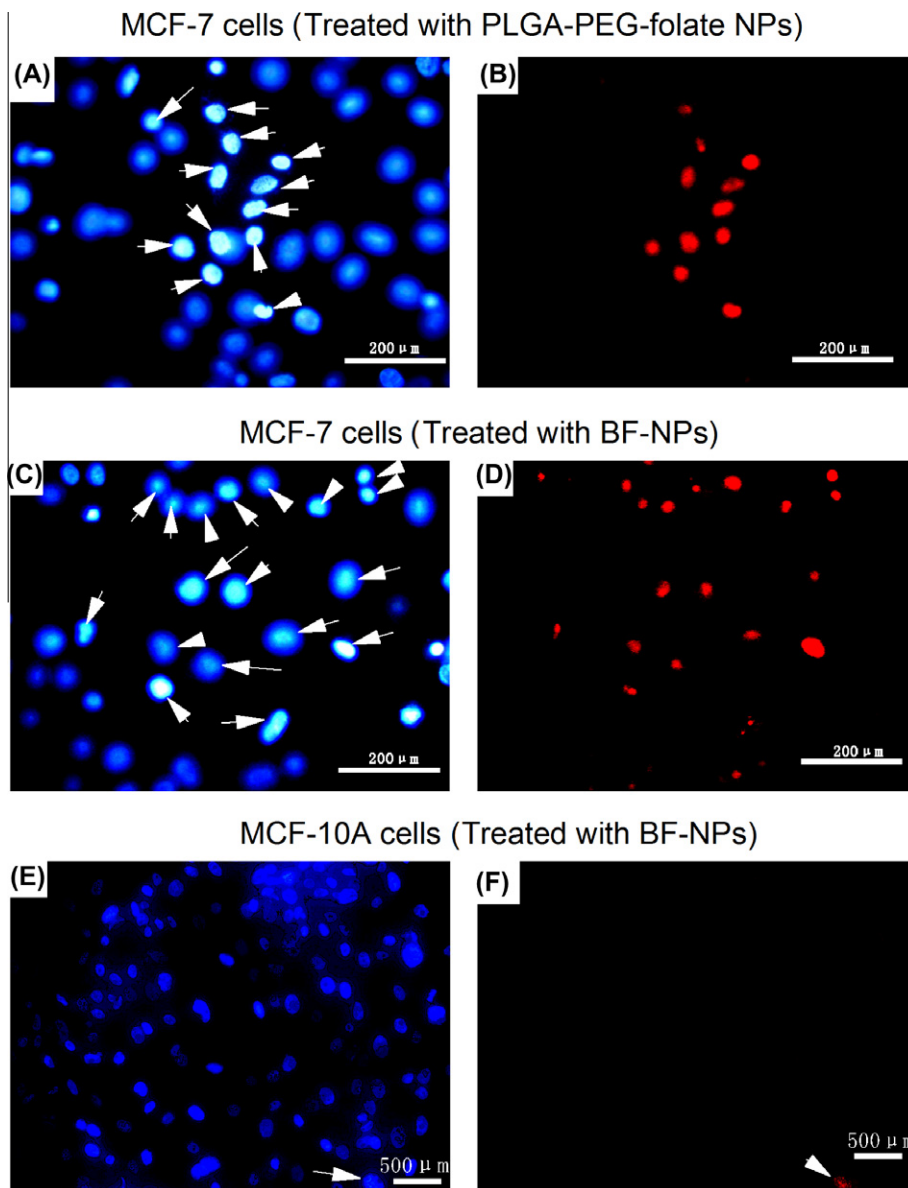


Fig. 10. Effects of VCR formulations on the morphology of MCF-7 cells (A–D) and MCF-10A cells (E and F). After the cells were co-incubated with VCR formulations for 12 h at 10 nM, they were washed with PBS and the nuclei were stained by incubating with Hoechst 33342 and PI for another 15 min in the darkness. Samples were observed under a fluorescence microscope. Figures (A), (C), and (E) were the fluorescence images of the cells stained with Hoechst 33342; figures (B), (D), and (F) were the fluorescence images of the cells stained with PI. Here only representative fluorescence micrographs were shown.

(Fig. 10B and D). This suggested that after 12 h exposure to VCR NPs, MCF-7 cells underwent the typical morphologic changes of apoptosis. However, after MCF-10A cells were treated with BF-NPs under the same conditions, only very pale red fluorescence was observed (Fig. 10F); the majority of MCF-10A cells kept their integrity and were only stained with Hoechst 33342 (Fig. 10E). These results indicated that under our experimental conditions, BF-NPs were more inclined to induce apoptosis in tumor cells MCF-7, but had a very limited effect on the normal cells MCF-10A.

3.7. Effects of BF-NPs on the cell cycle distribution in MCF-7 cells

To gain further insight into the mode of action of BF-NPs, we examined the effects of F-VCR and VCR NPs on the cell cycle by flow cytometry in MCF-7 cells. As shown in Fig. 11 and Table 4, DNA flow cytometric analysis indicated that treatment of MCF-7 cells with VCR formulations for 24 h significantly induced a G_2/M

phase arrest of the cell cycle. The percentage of cells with G_2/M phase was increased from $12.28 \pm 1.74\%$ (for the negative control, 0 nM), to above 33% (for F-VCR and VCR formulations, 10 nM). At the same time, the percentage of cells in the G_1 phase significantly decreased from $50.33 \pm 3.66\%$ (for the negative control) to below 25% (for VCR formulations, 10 nM). In Fig. 11, there was no significant difference ($p > 0.05$) in percentage of cells with G_2/M phase among the following groups at the same concentration (10 nM, according to the concentration of VCR): F-VCR (the positive control), PLGA-PEG-folate NPs, PLGA-PEG- R_7 NPs, and BF-NPs. This indicated that altered formulations of VCR (relative to F-VCR), such as nanoparticle formulations, did not lead to the change in the cell cycle arrest of MCF-7 cells if the concentration of VCR in the formulations was uniform. Moreover, cell apoptosis was detected simultaneously by apparent cell apoptosis peak. It has been reported that VCR belongs to cell cycle-specific drugs, which mainly arrests cell cycle at the G_2/M phase (Jordan et al., 1991). Exactly speaking,

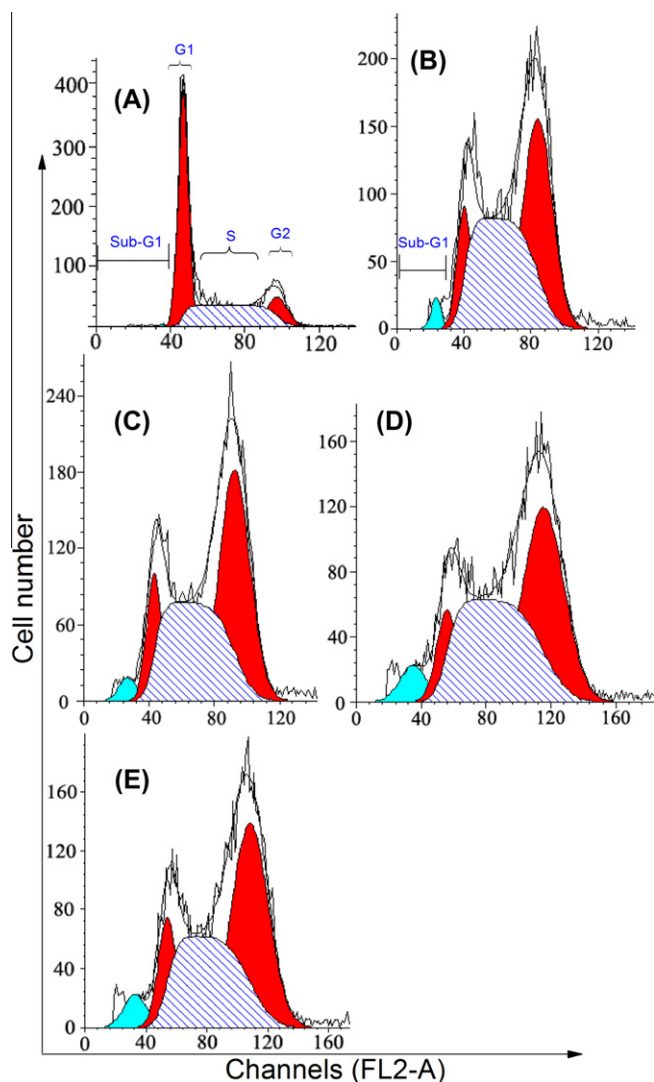


Fig. 11. Effects of VCR formulations (F-VCR and VCR NPs) on cell cycle progression in MCF-7 cells. Cells were incubated with 0 nM (histogram A) or 10 nM VCR formulations (histogram B–E) for 24 h and stained with PI. The DNA content was analyzed by fluorescence flow cytometry. Figures (B)–(E) represent the histograms of the cells treated with F-VCR, PLGA–PEG–folate NPs, PLGA–PEG–R₇ NPs, and BF-NPs, respectively. For each concentration, the cell cycle was conducted with three parallel samples; here only representative histograms were shown.

Table 4
Effects of VCR formulations (F-VCR or VCR NPs) on cell cycle arrest in MCF-7 cells.

Group	C (nM) ^a	G ₁ phase (%) ^b	S phase (%) ^b	G ₂ /M phase (%) ^b
Negative control	0	50.33 ± 3.66	37.39 ± 3.54	12.28 ± 1.74
F-VCR	10	23.44 ± 3.13 [*]	43.05 ± 5.05	33.51 ± 4.79 [*]
PLGA–PEG–folate NPs	10	20.94 ± 2.64 [*]	40.12 ± 3.69	38.94 ± 3.44 [*]
PLGA–PEG–R ₇ NPs	10	17.29 ± 3.34 [*]	46.17 ± 2.59	36.54 ± 2.95 [*]
BF-NPs	10	21.33 ± 2.54 [*]	39.66 ± 3.61	39.01 ± 3.74 [*]

^a Here refers to the concentration of VCR.

^b MCF-7 cells were treated with VCR formulations for 24 h and stained with PI. Cells treated with culture medium (untreated with VCR formulations) served as the negative control. The percentage of cell cycle (G₁ phase, S phase, and G₂/M phase) presented as mean ± SD (n = 3).

^{*} p < 0.05 versus the percentage of cells with G₁ phase (or G₂/M phase) of the negative control.

VCR arrests cell division at metaphase by the inhibition of formation of the mitotic spindle microtubulin (Himes et al., 1976; Binet et al., 1990; Ngan et al., 2000). Therefore, compared to F-VCR with the same concentration of VCR, BF-NPs also arrest the cell cycle in G₂/M phase.

After the chemotherapeutic agents are encapsulated into the NPs whose surfaces are modified with active targeting groups, their cytotoxicities significantly increase which is covered previously by several groups (Pan et al., 2010; Park et al., 2010; Yang et al., 2010b). However, the reason has not been fully figured out. From the above results, it's clear that there must be a correlation among the three aspects: the cellular uptake, cytotoxicity, and induced cell apoptosis. In our opinion, the process of the cytotoxicity generated by VCR NPs is successive and at least includes the following stages: (1) Internalization: In the first 1–4 h, VCR NPs pass through the tumor plasma membranes, then enter into the cytoplasm by endocytosis pathway, which is different from F-VCR; F-VCR enters into the cells by simple diffusion (Sahoo and Labhassetwar, 2005). PLGA–PEG–folate NPs loaded with VCR were delivered and then entered into tumor cells via folate receptor-mediated endocytosis pathway to a great extent; and the delivery of BF-NPs maybe depended on the synergism of folate receptor-mediated endocytosis and strong cell-penetrating power (Amand et al., 2008; Barz et al., 2010; Esmaeili et al., 2008). Moreover, the difference in internalization mechanisms between BF-NPs and F-VCR makes the former retain within the cells longer time; (2) VCR releases and cellular uptake reaches saturation: With the endocytosis in progress, VCR is released from the NPs and its concentration within the cells increases gradually. When the cellular concentration of VCR reaches a higher level, a plateau is reached (Zhang et al., 2010). That's to say, there is a saturated cellular uptake phenomenon of the NPs by MCF-7 cells. The above two processes maybe cost 2–6 h, and during this period the cellular uptake is dominant; (3) Apoptotic induction: Although the concentration of intracellular VCR has already reached a saturated level, it is still lower than that of extracellular VCR. The concentration drop makes the NPs loaded with VCR enter into the cells continuously. The further entry of the NPs and sustained high concentration of VCR within the cells lead to the supersaturated uptake, and then trigger the apoptosis of MCF-7 cells. From this moment, induced apoptosis gradually gains the upper hand. In the experiment, it was found that a number of MCF-7 cells no longer maintained their membrane integrity and some were divided into small pieces after 8 h or longer time's incubation with VCR-loaded BF-NPs. This result suggests that prolonged incubation time leads to the increase of the apoptotic cells. Cytotoxic compounds can exert their cytotoxic effect through multiple modes including the induction of necrosis, apoptosis, cell cycle arrest, and so on. As described above, DNA flow cytometric analysis indicated that treatment of MCF-7 cells with BF-NPs significantly induced a G₂/M phase arrest. Therefore, the G₂/M phase arrest of the cell cycle can be considered as another mode to suppress the growth of MCF-7 cells. From the above results combining with the previous studies, we believe that both of induced cell apoptosis and cell cycle arrest are two important modes by which VCR NPs exert their cytotoxic effect. Compared to F-VCR and another two kinds of VCR NPs at the same concentration, BF-NPs loaded with VCR are more effective.

4. Conclusion

Folate- and R₇-modified PLGA–PEG bifunctional NPs loaded with VCR, namely BF-NPs, were successfully prepared. Due to folate targeting function and obtained cell-penetrating power, BF-NPs demonstrated a superior cellular uptake to PLGA–PEG–folate NPs and PLGA–PEG–R₇ NPs. The enhanced cellular uptake of

BF-NPs directly results in stronger induction of apoptosis in MCF-7 cells; besides the cell cycle arrest at the G₂/M phase, the cell apoptotic induction is possible pathway by which PLGA-PEG NPs loaded with VCR exert their cytotoxic effect. Low cytotoxicity and weak ability to induce apoptosis in normal cells MCF-10A verified the excellent selectivity of the prepared BF-NPs. However, the above hypothesis is required to give an explanation in more detail using more experiments. The strong cell-penetrating power, enhanced cellular uptake, and an increased cytotoxicity by cell-penetrating peptide-modified NPs need to be elucidated from its mechanism. The further study to verify the above hypotheses is in progress.

Acknowledgments

This work was supported by the National Natural Science Foundation of China (Grant No. 30973644), the National Basic Research Program of China (973 Program), No. 2007CB936004, the key project of Guangxi Normal University (No. 2011ZD006), and the State Key Laboratory Cultivation Base for the Chemistry and Molecular Engineering of Medicinal Resources, Ministry of Science and Technology of China (CHEMR2012-A01).

References

- Amand, H.L., Fant, K., Norden, B., Esbjorner, E.K., 2008. Stimulated endocytosis in penetration uptake: effect of arginine and lysine. *Biochem. Biophys. Res. Commun.* 371, 621–625.
- Aroui, S., Brahim, S., Waard, M.D., Kenani, A., 2010. Cytotoxicity, intracellular distribution and uptake of doxorubicin and doxorubicin coupled to cell-penetrating peptides in different cell lines: a comparative study. *Biochem. Biophys. Res. Commun.* 391, 419–425.
- Barz, M., Canal, F., Koynov, K., Zentel, R., Vicent, M.J., 2010. Synthesis and in vitro evaluation of defined HPMA folate conjugates: influence of aggregation on folate receptor (FR) mediated cellular uptake. *Biomacromolecules* 11, 2274–2282.
- Bedikian, A.Y., Silverman, J.A., Papadopoulos, N.E., Kim, K.B., Hagey, A.E., Vardeleon, A., Hwu, W.J., Homsy, J., Davies, M., Hwu, P., 2011. Pharmacokinetics and safety of Marqibo (vincristine sulfate liposomes injection) in cancer patients with impaired liver function. *J. Clin. Pharmacol.* 51, 1205–1212.
- Binet, S., Chaineau, E., Fellous, A., Lataste, H., Krikorian, A., Couzinier, J.P., Meininger, V., 1990. Immunofluorescence study of the action of navelbine, vincristine and vinblastine on mitotic and axonal microtubules. *Int. J. Cancer* 46, 262–266.
- Chugh, A., Eudes, F., Shim, Y.S., 2010. Cell-penetrating peptides: nanocarrier for macromolecule delivery in living cells. *IUBMB Life* 62, 183–193.
- Cohen-Sela, E., Teitlboim, S., Chorny, M., Koroukhov, N., Danenberg, H.D., Gao, J., Golomb, G., 2009. Single and double emulsion manufacturing techniques of an amphiphilic drug in PLGA nanoparticles: formulations of mithramycin and bioactivity. *J. Pharm. Sci.* 98, 1452–1462.
- Cun, D., Foged, C., Yang, M., Frokjaer, S., Nielsen, H.M., 2010. Preparation and characterization of poly(DL-lactide-co-glycolide) nanoparticles for siRNA delivery. *Int. J. Pharm.* 390, 70–75.
- Danhier, F., Ansorena, E., Silva, J.M., Coco, R., Le Breton, A., Préat, V., 2012. PLGA-based nanoparticles: an overview of biomedical applications. *J. Controlled Release*. <http://dx.doi.org/10.1016/j.jconrel.2012.01.043>.
- Davda, J., Labhasetwar, V., 2002. Characterization of nanoparticle uptake by endothelial cells. *Int. J. Pharm.* 233, 51–59.
- Desai, P., Patlolla, R.R., Singh, M., 2010. Interaction of nanoparticles and cell-penetrating peptides with skin for transdermal drug delivery. *Mol. Membr. Biol.* 27, 247–259.
- El-Sayed, A., Futaki, S., Harashima, H., 2009. Delivery of macromolecules using arginine-rich cell-penetrating peptides: ways to overcome endosomal entrapment. *AAPS J.* 11, 13–22.
- Esmaili, F., Ghahremani, M.H., Ostad, S.N., Atyabi, F., Seyedabadi, M., Malekshahi, M.R., Amini, M., Dinarvand, R., 2008. Folate-receptor-targeted delivery of docetaxel nanoparticles prepared by PLGA-PEG-folate conjugate. *J. Drug Target.* 16, 415–423.
- Fonseca, S.B., Pereira, M.P., Kelley, S.O., 2009. Recent advances in the use of cell-penetrating peptides for medical and biological applications. *Adv. Drug Delivery Rev.* 61, 953–964.
- Gan, C.W., Feng, S.S., 2010. Transferrin-conjugated nanoparticles of poly(lactide)-D- α -tocopheryl polyethylene glycol succinate diblock copolymer for targeted drug delivery across the blood-brain barrier. *Biomaterials* 31, 7748–7757.
- Goncalves, E., Kitas, E., Seelig, J., 2005. Binding of oligoarginine to membrane lipids and heparan sulfate: structural and thermodynamic characterization of a cell-penetrating peptide. *Biochemistry* 44, 2692–2702.
- Herbig, M.E., Weller, K.M., Merkle, H.P., 2007. Reviewing biophysical and cell biological methodologies in cell-penetrating peptide (CPP) research. *Crit. Rev. Ther. Drug Carrier Syst.* 24, 203–255.
- Herce, H.D., Garcia, A.E., Litt, J., Kane, R.S., Martin, P., Enrique, N., Rebolledo, A., Milesi, V., 2009. Arginine-rich peptides destabilize the plasma membrane, consistent with a pore formation translocation mechanism of cell-penetrating peptides. *Biophys. J.* 97, 1917–1925.
- Himes, R.H., Kersey, R.N., Heller-Bettinger, I., Samson, F.E., 1976. Action of the vinca alkaloids vincristine, vinblastine, and desacetyl vinblastine amide on microtubules in vitro. *Cancer Res.* 36, 3798–3802.
- Hu, K., Li, J., Shen, Y., Lu, W., Gao, X., Zhang, Q., Jiang, X., 2009. Lactoferrin-conjugated PEG-PLA nanoparticles with improved brain delivery: in vitro and in vivo evaluations. *J. Controlled Release* 134, 55–61.
- Jordan, M.A., Thrower, D., Wilson, L., 1991. Mechanism of inhibition of cell proliferation by Vinca alkaloids. *Cancer Res.* 51, 2212–2222.
- Kassem, L.A., Gamal El-Din, M.M., Yassin, N.A., 2011. Mechanisms of vincristine-induced neurotoxicity: possible reversal by erythropoietin. *Drug Discovery Ther.* 5, 136–143.
- Maiolo, J.R., Ferrer, M., Ottinger, E.A., 2005. Effects of cargo molecules on the cellular uptake of arginine-rich cell-penetrating peptides. *Biochim. Biophys. Acta* 1712, 161–172.
- Marinina, J., Shenderova, A., Mallory, S.R., Schwendeman, S.P., 2000. Stabilization of vinca alkaloids encapsulated in poly(lactide-co-glycolide) microspheres. *Pharm. Res.* 17, 677–683.
- Marty, C., Meylan, C., Schott, H., Ballmer-Hofer, K., Schwendener, R.A., 2004. Enhanced heparan sulfate proteoglycan-mediated uptake of cell-penetrating peptide-modified liposomes. *Cell. Mol. Life Sci.* 61, 1785–1794.
- Mena-Rejon, G., Caamal-Fuentes, E., Cantillo-Ciau, Z., Cedillo-Rivera, R., Flores-Guido, J., Moo-Puc, R., 2009. In vitro cytotoxic activity of nine plants used in Mayan traditional medicine. *J. Ethnopharmacol.* 121, 462–465.
- Meng, F.T., Ma, G.H., Qiu, W., Su, Z.G., 2003. W/O/W double emulsion technique using ethyl acetate as organic solvent: effects of its diffusion rate on the characteristics of microparticles. *J. Controlled Release* 91, 407–416.
- Nahar, M., Dubey, V., Mishra, D., Mishra, P.K., Dube, A., Jain, N.K., 2010. In vitro evaluation of surface functionalized gelatin nanoparticles for macrophage targeting in the therapy of visceral leishmaniasis. *J. Drug Target.* 18, 93–105.
- Ngan, V.K., Bellman, K., Panda, D., Hill, B.T., Jordan, M.A., Wilson, L., 2000. Novel actions of the antitumor drugs vinflunine and vinorelbine on microtubules. *Cancer Res.* 60, 5045–5051.
- Noble, C.O., Guo, Z., Hayes, M.E., Marks, J.D., Park, J.W., Benz, C.C., Kirpotin, D.B., Drummond, D.C., 2009. Characterization of highly stable liposomal and immunoliposomal formulations of vincristine and vinblastine. *Cancer Chemother. Pharmacol.* 64, 741–751.
- Pan, J., Liu, Y., Feng, S.S., 2010. Multifunctional nanoparticles of biodegradable copolymer blend for cancer diagnosis and treatment. *Nanomedicine* 5, 347–360.
- Park, S., Kang, S., Veach, A.J., Vedvyas, Y., Zarnegar, R., Kim, J.Y., Jin, M.M., 2010. Self-assembled nanoplatform for targeted delivery of chemotherapy agents via affinity-regulated molecular interactions. *Biomaterials* 31, 7766–7775.
- Patel, L.N., Zaro, J.L., Shen, W.C., 2007. Cell penetrating peptides: intracellular pathways and pharmaceutical perspectives. *Pharm. Res.* 24, 1977–1992.
- Patlolla, R.R., Desai, P.R., Belay, K., Singh, M.S., 2010. Translocation of cell penetrating peptide engrafted nanoparticles across skin layers. *Biomaterials* 31, 5598–5607.
- Richard, J.P., Melikov, K., Brooks, H., Prevot, P., Lebleu, B., Chernomordik, L.V., 2005. Cellular uptake of unconjugated TAT peptide involves clathrin-dependent endocytosis and heparan sulfate receptors. *J. Biol. Chem.* 280, 15300–15306.
- Sahoo, S.K., Labhasetwar, V., 2005. Enhanced antiproliferative activity of transferrin-conjugated paclitaxel-loaded nanoparticles is mediated via sustained intracellular drug retention. *Mol. Pharm.* 2, 373–383.
- Schmidt, N., Mishra, A., Lai, G.H., Wong, G.C., 2010. Arginine-rich cell-penetrating peptides. *FEBS Lett.* 584, 1806–1813.
- Sethuraman, V.A., Lee, M.C., Bae, Y.H., 2008. A biodegradable pH-sensitive micelle system for targeting acidic solid tumors. *Pharm. Res.* 25, 657–666.
- Shimazawa, M., Ito, Y., Inokuchi, Y., Hara, H., 2007. Involvement of double-stranded RNA-dependent protein kinase in ER stress-induced retinal neuron damage. *Invest. Ophthalmol. Vis. Sci.* 48, 3729–3736.
- Skladanowski, A., Come, M.G., Sabisz, M., Escargueil, A.E., Larsen, A.K., 2005. Down-regulation of DNA topoisomerase II α leads to prolonged cell cycle transit in G2 and early M phases and increased survival to microtubule-interacting agents. *Mol. Pharmacol.* 68, 625–634.
- Stella, B., Marsaud, V., Arpicco, S., Geraud, G., Cattel, L., Couvreur, P., Renoir, J.M., 2007. Biological characterization of folic acid-conjugated poly(H2NPEGCA-co-HDCA) nanoparticles in cellular models. *J. Drug Target.* 15, 146–153.
- Su, Y., Waring, A.J., Ruchala, P., Hong, M., 2010. Membrane-bound dynamic structure of an arginine-rich cell-penetrating peptide, the protein transduction domain of HIV TAT, from solid-state NMR. *Biochemistry* 49, 6009–6020.
- Thoren, P.E., Persson, D., Lincoln, P., Norden, B., 2005. Membrane destabilizing properties of cell-penetrating peptides. *Biophys. Chem.* 114, 169–179.
- Torchilin, V.P., 2008. Cell penetrating peptide-modified pharmaceutical nanocarriers for intracellular drug and gene delivery. *Biopolymers* 90, 604–610.
- Tseng, Y.L., Liu, J.J., Hong, R.L., 2002. Translocation of liposomes into cancer cells by cell-penetrating peptides penetration and tat: a kinetic and efficacy study. *Mol. Pharmacol.* 62, 864–872.

- van Vlerken, L.E., Vyas, T.K., Amiji, M.M., 2007. Poly(ethylene glycol)-modified nanocarriers for tumor-targeted and intracellular delivery. *Pharm. Res.* 24, 1405–1414.
- Wang, M., Thanou, M., 2010. Targeting nanoparticles to cancer. *Pharmacol. Res.* 62, 90–99.
- Wang, Z., Chui, W.-K., Ho, P., 2009. Design of a multifunctional PLGA nanoparticulate drug delivery system: evaluation of its physicochemical properties and anticancer activity to malignant cancer cells. *Pharm. Res.* 26, 1162–1171.
- Wang, J.F., Liu, W.M., Tu, Q., Wang, J.C., Song, N., Zhang, Y.R., Nie, N., Wang, J.Y., 2011. Folate-decorated hybrid polymeric nanoparticles for chemically and physically combined paclitaxel loading and targeted delivery. *Biomacromolecules* 228, 228–234.
- Wang, S.P., Chen, T.K., Chen, R., Hu, Y.Y., Chen, M.W., Wang, Y.T., 2012. Emodin loaded solid lipid nanoparticles: preparation, characterization and antitumor activity studies. *Int. J. Pharm.* 430, 238–246.
- Win, K.Y., Feng, S.S., 2005. Effects of particle size and surface coating on cellular uptake of polymeric nanoparticles for oral delivery of anticancer drugs. *Biomaterials* 26, 2713–2722.
- Wu, L., Tang, C., Yin, C., 2010. Folate-mediated solid-liquid lipid nanoparticles for paclitaxel-coated poly(ethylene glycol). *Drug Dev. Ind. Pharm.* 36, 439–448.
- Yang, S.J., Lin, F.H., Tsai, K.C., Wei, M.F., Tsai, H.M., Wong, J.M., Shieh, M.J., 2010a. Folic acid-conjugated chitosan nanoparticles enhanced protoporphyrin IX accumulation in colorectal cancer cells. *Bioconjugate Chem.* 21, 679–689.
- Yang, X., Grailer, J.J., Rowland, I.J., Javadi, A., Hurley, S.A., Steeber, D.A., Gong, S., 2010b. Multifunctional SPIO/DOX-loaded wormlike polymer vesicles for cancer therapy and MR imaging. *Biomaterials* 31, 9065–9073.
- Yoo, H.S., Park, T.G., 2004. Folate receptor targeted biodegradable polymeric doxorubicin micelles. *J. Controlled Release* 96, 273–283.
- Zhang, P., Hu, L., Wang, Y., Wang, J., Feng, L., Li, Y., 2010. Poly(ϵ -caprolactone)-block-poly(ethylene phosphate) micelles for brain-targeting drug delivery: in vitro and in vivo valuation. *Pharm. Res.* 27, 2657–2669.
- Zhu, G., Mallery, S.R., Schwendeman, S.P., 2000. Stabilization of proteins encapsulated in injectable poly (lactide-co-glycolide). *Nat. Biotechnol.* 18, 52–57.
- Ziegler, A., Blatter, X.L., Seelig, A., Seelig, J., 2003. Protein transduction domains of HIV-1 and SIV TAT interact with charged lipid vesicles. Binding mechanism and thermodynamic analysis. *Biochemistry* 42, 9185–9194.